1-25-2022

Modeling defect mediated color-tunability in LEDs with Eu-doped GaN-based active layers

Hayley J. Austin

Brandon Mitchell

Dolf Timmerman

Jun Tatebayashi

Shuhei Ichikawa

See next page for additional authors

Authors

Hayley J. Austin, Brandon Mitchell, Dolf Timmerman, Jun Tatebayashi, Shuhei Ichikawa, Yasufumi Fujiwara, and Volkmar Dierolf

Journal of Applied Physics

Modeling defect mediated color-tunability in LEDs with Eu-doped GaN-based active layers

Cite as: J. Appl. Phys. **131**, 045701 (2022); https://doi.org/10.1063/5.0077223
Submitted: 31 October 2021 • Accepted: 10 January 2022 • Published Online: 25 January 2022

Hayley J. Austin, Brandon Mitchell, Dolf Timmerman, et al.

Journal of Applied Physics ARTICLE scitation.org/journal/jap

Modeling defect mediated color-tunability in LEDs with Eu-doped GaN-based active layers

Cite as: J. Appl. Phys. **131**, 045701 (2022); doi: 10.1063/5.0077223
Submitted: 31 October 2021 · Accepted: 10 January 2022 ·
Published Online: 25 January 2022

Hayley J. Austin,[1,a)] Brandon Mitchell,[1,2,3] Dolf Timmerman,[3] Jun Tatebayashi,[3] Shuhei Ichikawa,[3] Yasufumi Fujiwara,[3] and Volkmar Dierolf[1]

AFFILIATIONS

[1]Department of Physics, Lehigh University, Bethlehem, Pennsylvania 18015, USA
[2]Department of Physics, West Chester University, West Chester, Pennsylvania 19383, USA
[3]Division of Materials and Manufacturing Science, Graduate School of Engineering, Osaka University, 2-1 Yamadaoka, Suita, Osaka 565-0871, Japan

Note: This paper is part of the Special Topic on Defects in Semiconductors.
[a)]**Author to whom correspondence should be addressed:** hja218@lehigh.edu

ABSTRACT

Color tunability from red to orange to yellow has been demonstrated in GaN-based LED devices with Eu-doped GaN layers as the active region. Under current injection, this is achieved by varying the current density and the pulse conditions. The underlying mechanism behind this color tunability is a redistribution of energy among the ^5D_J states of a Eu^{3+} ion. This energy shuffling is facilitated by a local defect that has been neglected in previous modeling work. Including this defect allows for a quantitative prediction of the relative time-averaged populations of the Eu^{3+} ion's $^5D_0$ and $^5D_1$ states. Extracting, from experimental results, the red and yellow/green emission spectra due to radiative transitions from the respective levels and mixing them allows the overall chromaticity of the emission to be determined for varied excitation conditions. In addition, the model allows us to determine the optimal injection conditions to maximize the gamut of color tunability while minimizing power consumption. These simulations pave the way for practical, systematic color tuning from a single-contact pixel.

INTRODUCTION

Colored LED lighting has many potential applications from standard, professional, and agricultural lighting to personal and commercial displays. Various biological impacts of artificial light are seen in the way that colored light can be used to facilitate mood and manipulate the growth and health of plants and animals.[1–3] These impacts are relevant to humans in a modern society as blue light can interfere with circadian rhythms. Now, because of health concerns, the design and usage of personal devices is being reevaluated.[4,5] LEDs are favored over alternative lighting methods due to their efficiency and stability.[6,7] Current display technology relies on combining single-colored subpixels that each have controllable intensity so that color mixing gives a desired net color for the pixel. To create such displays, efforts have been made to produce at least three emission colors in close proximity. Such manufacturing typically involves combining layers of InGaN or AlGaInP and utilizing heterostructures to achieve various colors. These structures are then monolithically integrated onto the same substrate, either by growing them together or by binding multiple, separately grown parts.[8–10] Though good color gamut and efficiency can be obtained with these RGB or RGBY displays, using three or four subpixels together requires a large amount of integration. This complicates device fabrication by initially requiring more complicated growth or binding techniques or involving the wiring of multiple pairs of contacts during post-production, all of which is costly and less efficient.

Several different techniques and material systems are being explored to realize a new generation of color-tunable LEDs. For GaN-based systems, InGaN quantum well (QW) LEDs have been shown to color tune with injection current density and pulse operating conditions.[11] To achieve red emission, the In content in the QWs was increased, which created V-shaped defects. The resulting blueshift due to band-filling and piezoelectric screening effects was then used to extend the tunability. The red emission was weaker

than the blue–green emission, so pulse conditions of the latter were adjusted to match the lower brightness of the red emission. Furthermore, the size of the LED had to be decreased to move the color toward blue, so the color tunability is not flexible within a single device.[11] Other groups have also focused on nanostructures; for example, Ag nanowire surface plasmons have been used to achieve ZnO/GaN color tunability from yellow–green to blue–violet emission. However, this report did not mention avenues to obtain tunability toward red.[12] In addition, hybridization of solid-state LEDs and organic LEDs (OLEDs) could be used to bridge color gaps. For example, horizontal integration resulted in the creation of a multifunctional tandem LED.[13] In this device, a yellow quantum dot (QD) LED, which mixed red and green quantum dots, was stacked on a blue OLED connected in parallel and was operated using AC injection. This device was able to produce RGB light and pure white light but still required two terminals and significant post-growth fabrication. Alternatively, Wang *et al.* demonstrated all OLED-based devices with a simpler structure that utilized a PN heterojunction as the emitting layer. These devices could color tune by starting at a point on the RY axis and moving toward blue, but different devices are needed for each point along the RY axis.[14]

In our research, we are working toward a GaN-based LED pixel that uses a single set of contacts, which allows for smaller individual pixels and avoids the problem of crosstalk among sub-pixels.[15] Reduced pixel size would benefit many technological endeavors, such as creating high-resolution micro-LED displays and smaller, wearable displays, such as those found in smartwatches.[16–18] Some single-contact color-tunable LEDs have been demonstrated. For example, quantum dot (QD) LEDs were fabricated by vertically stacking multiple QD layers to obtain various emission colors.[19] By taking advantage of a charge modulation layer, RY color tunability was found to be better-controlled and enhanced beyond typical QD tunability. However, extending the color tunability into the blue was not discussed. El-Ghoroury *et al.* used vertically stacked InGaN quantum wells to produce individual red, green, and blue emitting layers, each separated by AlGaN intermediate carrier blocking layers.[20] The result was a single-contact color-tunable LED that could also produce white light of varying warmness. While these LEDs had single-pixel color tunability, they required low current to obtain red emission, and thus the red emission was substantially weaker than the blue or green emission.

Our research focuses on using GaN doped with rare earth (RE) ions, as these ions produce stable and narrow emission at desired wavelengths.[21] Our current progress includes the monolithic growth of a vertically stacked RGB LED, where InGaN/GaN QWs are used to obtain the blue and green emission, and Eu-doped GaN is used for the red emission.[22] In this device, each color could be addressed and controlled individually. However, Eu-doped GaN-based LEDs alone show potential for single-contact full-color pixels. In a previous work, we have reported that by increasing the intensity of a continuous injected current, the emission from a Eu-doped GaN-based LED could be tuned from red at low current, through orange hues at intermediate currents, to yellow at high current.[23] Eu^{3+} ions are known to emit a bright red color at 622 nm due to the $^5D_0 \rightarrow {}^7F_2$ transition and can also emit green at 545 nm due to the $^5D_1 \rightarrow {}^7F_1$ transition. However, this green emission is typically much weaker in brightness than the red emission.[23,24] Two other transitions from the $^5D_1$ state to the $^7F_2$ and $^7F_3$ states result in green–yellow and yellow–orange emission, respectively. These latter two emissions can be suppressed with filters or through nanostructures for a purer green emission, and we are working on methods to selectively enhance green or other desired Eu emissions.[23–25] While Eu emission, as with the emission from all RE ions, is slow, it has the advantage of being spectrally stable against current injection. Thus, unlike the emission from conventional InGaN-based LEDs, injection current and temperature have a negligible effect on the position of the Eu emission peaks.[26]

Additional dopants can be used to obtain the blue emission necessary for full-color tunability. For example, our group has demonstrated that co-doping with Si and Mg led to color tunability from red to magenta under different current injection conditions.[23] The blue emission around 430 nm is broad and originates from a Si–Mg complex, which has also been observed in other Si/Mg co-doped GaN LEDs.[27] This additional blue emission makes it feasible for a single Eu-doped GaN active layer within an LED structure to have RGB tunability from a single contact.

For practical use of these devices, it is important to understand the impact of the current injection conditions on the emitted color, output power, and external quantum efficiency (EQE), which can be simulated using a model based on a set of rate equations. Previous rate equation simulations modeled the population changes as the energy moved between the Eu^{3+} ion levels, and a branching ratio determined the relative occupancy of the $^5D_2$ and the $^5D_0$ levels after initial excitation. These simulations yielded values of relative level occupancy that were qualitatively consistent with the emission intensity observed in electroluminescence (EL) experiments.[23] It was also noted that the color could be changed by varying the duty cycle under pulsed excitation. However, this previous model, which was based on a continuous injection current, could not explain the relationship between color trends and pulse frequency. To further explore avenues of color tunability, we extended these initial models by considering a local defect complex as a trap for carriers that transfer energy to the Eu^{3+} ion and performed simulations at various pulse sequences. The results from these models can help guide our experimental work as we aim to fabricate a single-pixel LED with full-color tunability.

METHODS

There are benefits in accounting for a local defect when modeling these systems. A defect local to the Eu^{3+} ion can facilitate certain excitation transfer processes by capturing charge carriers that then recombine in the vicinity of the Eu^{3+} ion, where different defects have different properties, but we are considering the population of a single, generic defect. One of the advantages of including a defect complex into our model is that in some cases, recombinations within the complex can produce their own characteristic emission, such as the blue emission observed from Si–Mg complexes in GaN.[27,28] Including this local defect in the model makes it more adaptable and able to account for radiative transitions from the Eu^{3+} ions and from the complex itself, which have both been

observed experimentally. Figure 1 outlines the general excitation process and the role of a local defect complex. A rate equation approach is taken to model the excitation process shown in Fig. 1, which explicitly includes the local defect. This local defect is described as a system that can be in two different states: a ground state with a population (m_0) and an excited state (m_1) from which excitation transfer can occur. The Eu^{3+} ion is simplified as a three-level system with the ground states $^7F_{0-6}$ considered together as ^7F, and the two excited states, $^5D_0$ and $^5D_1$. Though energy can be transferred to the $^5D_2$ state from the defect, it is omitted from this model due to its fast decay time (within 0.1 μs at room temperature) into the $^5D_1$.[29] Instead, the energy is modeled as being transferred directly into the $^5D_1$ state.

In the model, we are considering excitation, re-excitation, and decays. Energy pumped into the system through carrier injection causes m_1 to become populated. The defect may send energy into the Eu^{3+} ion, causing excitation of the ion and depopulation of m_1. During "re-excitation," the Eu^{3+} ion decays and returns energy to the defect, which may, however, transfer the energy back to the Eu^{3+} ion, allowing for the ion to become excited again but into a different level. The decays we are monitoring are transitions within the Eu^{3+} ion. The net transitions are displayed in Fig. 2 and are color-coded by type,

$$\frac{\partial n_{D_1}}{\partial t} = m_1 y(n_F + n_{D_0}) - m_1 x n_{D_1} - n_{D_1} k_1,$$
$$\frac{\partial n_{D_0}}{\partial t} = m_1 x(n_F + n_{D_1}) - m_1 y n_{D_0} - n_{D_0} k_0 + n_{D_1} k_1,$$
$$\frac{\partial n_F}{\partial t} = -m_1(x+y)n_F + n_{D_0} k_0,$$
$$\frac{\partial m_1}{\partial t} = \frac{I}{n_{Eu}} m_0 - m_1(x+y)(n_{D_0} + n_{D_1} + n_F).$$

The increase in populations due to excitations depends on the corresponding transfer rate, x or y, which are the rates into $^5D_0$ and $^5D_1$ states, respectively. Experiments have shown these transfer rates to be approximately equal. For this work, $x = y = 10^{10}\ s^{-1}$ was chosen as it corresponds to a 100 ps timescale, which is relevant because Eu^{3+} ion-related emission is seen within 100 ps of excitation and carrier capture due to Eu^{3+} traps occurs after ~85 ps.[30]

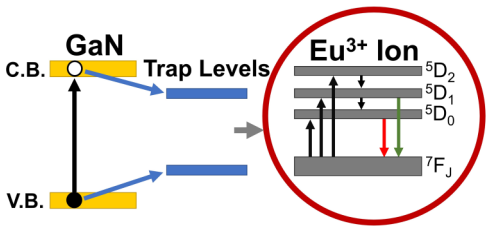

FIG. 1. Model for the energy transfer process of carriers generated in GaN to the Eu^{3+} ions. The excitation process is as follows: when electrons move from the valence band into the conduction band, some energy may be captured by electron and hole traps, which are defects local to the Eu^{3+} ion. Electrons and holes then recombine and transfer their energy via an Auger process to the Eu^{3+} ion, where transitions between states can emit radiatively.

Decays within the 4*f* manifold of the Eu^{3+} ions occur more slowly. The $^5D_1$ state decays into the $^5D_0$ state with transition rate k_1, and $^5D_0$ decays into ^7F with transition rate k_0. From previous time-resolved photoluminescence experiments, we take $k_0 = 4 \times 10^3$ and $k_1 = 4 \times 10^5\ s^{-1}$.[23]

This model assumes that the radiative rates of emission from $^5D_0$ and $^5D_1$ are equal[23,29] and that the populations of these states are proportional to the amount of emitted light. Color can be inferred by looking at the ratio between the average steady-state values of n_{D0} and n_{D1}, using EL and photoluminescence spectra as color references. The primary emission from $^5D_0$ is a bright red with some minor peaks indicating some orange emission, while the $^5D_1$ state contributes relatively more yellow–green light.[23] Therefore, the ratio between $^5D_0$ and $^5D_1$ emission can be stated as the percent of the $^5D_0$ contribution. In this manner, 0% $^5D_0$ would result in a yellow–green color with a mixed contribution from the various $^5D_1$ state-related emissions, and 100% $^5D_0$ would yield a deep red color at ~622 nm.

To test and evaluate this model, a variety of simulations were performed and compared with EL experiments. In order to test for tunability at a constant excitation, simulations were performed at constant set intensity (I_{set}), where constant I_{set} is analogous to the constant injection current (I_{peak}) in EL experiments. Constant root mean square power (P_{rms}) simulations were performed to test for constant effective input, independent of the duty cycle. For these

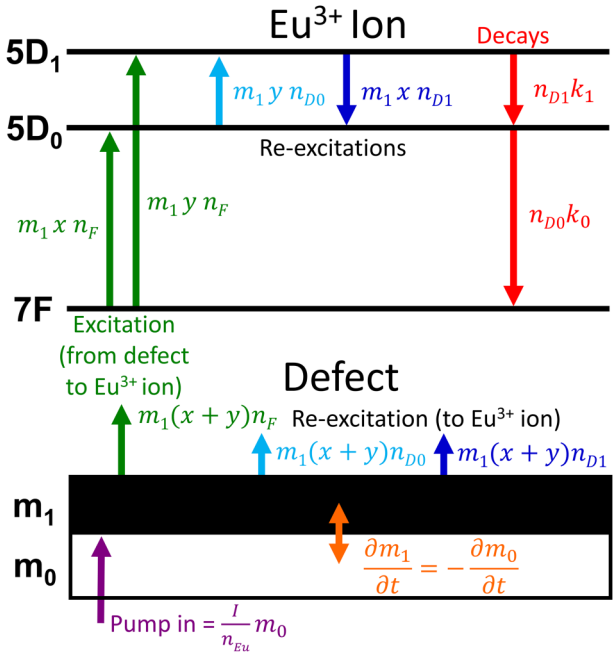

FIG. 2. Diagram of the transitions considered in the model, where the defect is considered as a two-level system and the Eu^{3+} ion as a three-level system. The Eu^{3+} ion-level populations are abbreviated as n_F, n_{D0}, and n_{D1}, and fractional populations are used so that a fully populated state has a population of 1 and $0 \le n, m \le 1$.

constant P_{rms} experiments, the intensity had to be increased at low duty cycles to compensate for the short pulse duration, which was done by varying I_{set} according to the relation

$$I_{set,\ duty\ cycle} = \frac{I_{set,50\%}}{2(duty\ cycle)}.$$

For simulations of duty cycles ranging from 5% to 95%, the intensity varied by a factor of ~20, similar to the current range used in EL experiments.[23]

Working toward a fully controllable display with continuous brightness, it would be desirable to be able to tune color while maintaining constant output power (P_{out}) and controlling the display's dimming. Typically, LEDs have been dimmed via digital or analog methods. For digital dimming, the current pulse width is modulated, while for analog dimming, the current density is adjusted.[31] To explore possible methods for tunability while controlling brightness, constant P_{out} simulations were performed. Constant P_{out} was defined as being in proportion to both I_{set} and the sum of the populations of the excited states,

$$P_{out} = I_{set}(n_{D_0} + n_{D_1}),$$

and effective intensity was defined as

$$I_{eff} = I_{set}(duty\ cycle),$$

in order to compare the amount of applied intensity, regardless of the time on due to duty cycle, which is useful in determining and comparing external quantum efficiency (EQE). EQE is defined as

$$EQE = \frac{(n_{D_0} + n_{D_1})k}{I_{eff}},$$

where $k = 5000\ s^{-1}$, the approximate emission rate from the Eu^{3+} ion. It should also be noted that in this definition of EQE, duty cycle is accounted for in the I_{eff} term.

RESULTS

In a series of EL experiments that varied the duty cycle but were performed with constant I_{peak}, increasing the duty cycle from 5% to 99.9% resulted in a color change trend of dark orange to yellow at 60 Hz [Fig. 3(b)]. At a higher frequency of 10 kHz, this effect was more dramatic, moving from dark red through orange and then to yellow as the duty cycle was increased. Simulations shown in Fig. 3(a) have comparable results. Simulations with constant I_{set} showed a more moderate color shift of orange to lighter orange at 60 Hz, while at 10 kHz, there was a more substantial color change of red through to light orange.

Experiments performed at constant P_{rms} and low frequency (60 Hz) showed that color moved from yellow to red color when increasing the duty cycle from 5% to 99.9%. The simulations predicted a similar light orange to red color change. Simulations at the higher frequency of 10 kHz suggest the reverse behavior of a strong red to orange change.

A series of constant P_{out} simulations, shown in Fig. 4(a), were performed with the high output power value of $(1.000 \pm 0.005) \times 10^7\ s^{-1}$. At lower frequencies between 10 Hz and 10 kHz, highlighted in gray, the color tunability occupied the same regime in a way that is not significantly dependent on frequency. There, $^5D_0$ populations suggest red colors at the lower duty cycles, which move toward orange at higher duty cycles. At higher frequencies, from 10 kHz up to 10 MHz, frequency-dependent color tunability was achieved at a constant duty cycle, where the 10 kHz data predicted red and moved toward orange as frequency approached 10 MHz. This effect is seen clearly for the 5% and 10% duty cycles (circled in blue and green, respectively) and required relatively low intensities to achieve. The same color change is also seen at the 1% duty cycle (circled in purple), though intensity must be slightly adjusted, by a factor of ~3, in order to reach the same levels of tunability at constant P_{out}.

Comparing the calculated EQEs for constant $P_{out} = 1 \times 10^7$, shown in Fig. 4(b), the 100 kHz run at 1% duty cycle had the best EQE of 4.6%, which decreased to 1.0% for a duty cycle of 5%. Results from frequencies between 10 kHz and 1 MHz gave rise to EQEs between 2.0% and 4.6% at duty cycle = 1% and EQEs between 0.71% and 1.0% at duty cycle = 5%. Frequencies $\geq$ 10 MHz and $\leq$ 1 kHz had EQEs below 0.5%, even at a low duty cycle.

DISCUSSION

Since these new simulations can model pulsed excitation, they can provide a quantitative explanation for the previously seen color trends from pulsed EL experiments. For EL experiments with constant I_{peak}, the emitted color always moves in the direction of yellow at higher duty cycles due to the lower ratio of $^5D_0$ to $^5D_1$. This shift is more pronounced at higher modulation frequencies, where low duty cycle simulations showed a very high percentage $^5D_0$ (red) as opposed to the orange color obtained for lower frequencies. This difference in color range is due to the nature of the pulse arrival times and widths, which differ at high and low frequencies. At 10 kHz, pulses arrive every 100 μs, while at 60 Hz, pulses arrive less frequently, every 16.6 ms. The short, frequent pulses of 10 kHz experiments allow for a dark red to be obtained at a low duty cycle due to the shorter gaps between pulses, which is short enough that the $^5D_0$ remains partially populated, weighing emission toward a red color and preventing yellow $^5D_1$ emission from having a large contribution. At a low duty cycle and a frequency of 60 Hz, having less frequent pulses gives the system time to relax and release more yellow emission. During this relaxation, there is enough time between pulse arrivals so that both the $^5D_0$ and $^5D_1$ states completely decay, and the relative population averages predict an orange color rather than the red seen at 10 kHz. For both low and high frequencies, as the duty cycle increases, the pulses are on for longer than they are off. Thus, excitation becomes similar to continuous excitation, where color moves from red to yellow for increased intensity. At high duty cycle, a similar pattern toward yellow was seen in both of the constant I_{set} cases.

For constant P_{rms}, it was already seen experimentally that, at low frequency, color shifts from yellow to red with an increase of duty cycle. This is because a higher intensity is required at lower duty cycles to obtain the constant P_{rms} value. This higher intensity

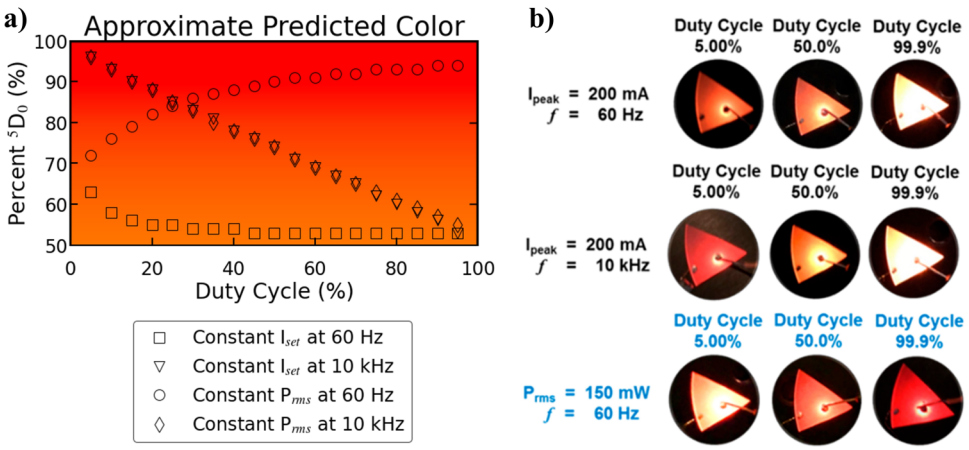

FIG. 3. Comparison of simulations at various duty cycles and selected I_{set} values with experimental results. (a) Selected simulations at constant I_{set} and constant P_{rms}. The color within the graph represents the expected color output of the LED, which is calculated based on the relative $^5D_0$ population. (b) Images of LED devices electrically excited with the noted parameters. Reprinted (adapted) with permission from Mitchell *et al.*, ACS Photonics **6**, 1153 (2019). Copyright 2019 American Chemical Society.

results in excitation conditions that lead to the yellow color. However, when pulses are delivered at higher frequencies, our simulations exhibited the reverse trend. Though experimental confirmation of this high-frequency constant P_{rms} excitation condition is in process, the more frequent pulses should supply enough energy that yellow emission would be expected at higher duty cycles. This result is similar to what was observed in both the low and high-frequency cases at constant I_{set}. Overall, this confirmation suggests that our model is functional for our purposes and reliable for further exploration.

To explore how this model can be used to develop a practical LED, constant P_{out} simulations were performed, and EQE values were calculated. Typically, continuous excitation is considered for conventional LED operations. However, we are considering pulsed excitation in our EQE simulations to take advantage of the unique optical properties of our devices. There were notable color trends at lower duty cycles, which had higher EQE values. It follows that operating a device at a lower duty cycle should be more efficient as the intensity (current) is on for a shorter period of time; thus, less energy is wasted. This behavior is particular to our devices because the emission timescales are slow. After sufficient current is applied within a certain pulse duration, additional current does not lead to further excitation since the Eu ions are saturated. It can be seen in the calculated EQE values of the constant P_{out} simulations that as the frequency was increased, the EQE was seen to increase and later decrease. Noting the timescales at which this change occurs, it follows that this increase is from nearing the maximum population of excited states, and the subsequent decrease in EQE is due to diminishing returns from increasing the intensity beyond what is needed for excitation. In addition, the pulse durations are too short at frequencies above 1 MHz to reach a maximum population of the excited states. Simulations with frequencies ranging from 10 through 400 kHz exhibited higher EQE values, where these frequencies correspond to 10^{-4} to $2.5 \times 10^{-6}\,s^{-1}$, which are on the order of the excited state lifetimes. Changing the frequency rather than intensity to tune color while maintaining constant P_{out} would allow for the intensity to be used to fine-tune the brightness or for analog dimming. It is also of note that by using more efficient pulse conditions, EQE could be increased, rather than just increasing EQE by optimizing device growth conditions. Thus, finding optimal pulse conditions would provide powerful controllability for device applications.

Moving forward, we are using our model and simulation results in order to design new devices with better tunability.

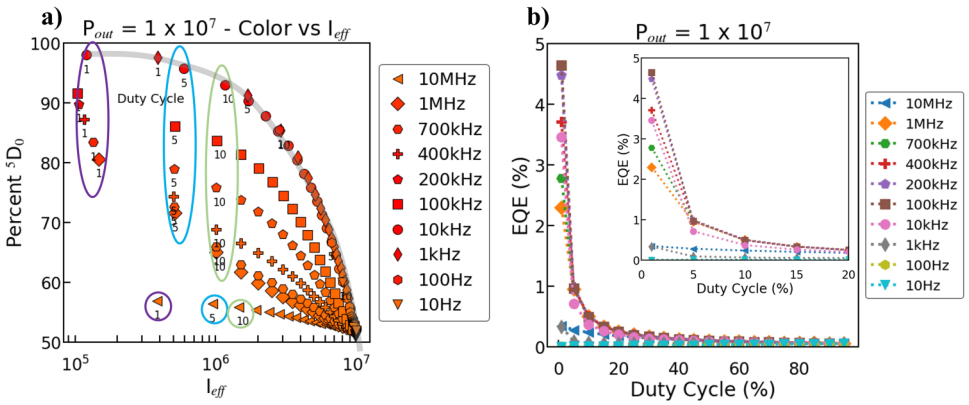

FIG. 4. (a) Simulations at constant $P_{out} = 1 \times 10^7$, colored based on the ratio between the $^5D_0$ and $^5D_1$ populations. Low-frequency results are clustered together and highlighted in gray. High-frequency runs at a duty cycle of 1% are circled in purple, 5% are circled in blue, and 10% are circled in green. (b) Calculated EQEs of the same constant P_{out} simulations, and the inset contains the same data but zoomed in on low duty cycle data.

Nanostructures show particular promise, as we have been able to enhance and filter the 545 nm green emission from the $^5D_1$ transition through the use of distributed Bragg reflectors.[24] Additionally, radiative lifetimes can be shortened, and thus, the radiative rate of $^5D_0$ emission can be enhanced via microdisk nanostructures due to coupling to whispering gallery modes.[24,25] By using Eu-doped GaN as the active layer, Si–Mg as a co-dopant for blue emission, and nanostructures to selectively enhance certain emission lines, we could potentially have sharp RGB peaks all in a single-pixel device.

Thus far, only Si–Mg defect complexes have produced significant emission that can be accessed along with the Eu emission.[23,27] Typically, in high-quality Eu-doped GaN, the emission from the Eu ions dominates, and band edge, exitonic, and other common defect emission lines are completely absent.[26] Other defects such as oxygen and Mg alone have been shown to enhance Eu incorporation and emission; however, they have not yet been shown to produce their own emission lines in our samples.[26,32] Luminescence from extended defects such as stacking faults has also been observed in GaN doped with Mg.[33] In this regard, it has been found that Eu atoms tend to accumulate around dislocations, which results in energy transfer to the Eu ions even in the presence of non-radiative decay channels and reduces the negative influence of dislocation and faults on the overall emission efficiency.[34] This does not mean that other dopants or growth conditions that introduce additional radiative channels cannot be found or explored. In the future, our model could allow us to predict the behavior of Eu-doped GaN devices containing other radiative defects if we know the emission wavelength and radiative lifetime of the defect.

CONCLUSION

In our newly developed model, the local defect is simulated as a mitigator of energy transfer. Incorporating the defect into our model allows for increased flexibility in simulations, as pulsed excitation can be modeled, and the population of the local defect itself can be monitored. Constant I_{set} and constant P_{rms} simulations predicted color in a way that explained previous experimental results. After this confirmation, the model was further used to predict other avenues of potential color tunability that offer applicability to practical devices. In simulations at constant output power, frequency-dependent red to orange color tunability was found while maintaining a constant duty cycle, requiring only minor adjustments to I_{set}. Most notably, this was possible at low duty cycle values, which have higher calculated EQE values than the higher duty cycle counterparts.

The simulations performed thus far show tunability along the R to G color axis. Moreover, we find that the same population ratios for $^5D_1$ and $^5D_0$ can be achieved with different combinations of frequency and duty cycle parameters. In other words, the same color on the R–G scale can be achieved various ways. Comparing the relative population of the excited trap state for these cases in existing simulations, we find that the $m_1/^5D_0$ population ratio can be varied by a factor of at least nine. Assuming that the trap releases a blue radiative decay, this would allow for tunability that spans the other direction color space, allowing for full RGB tunability in a single device. Since the population of the trap state is always much lower than in the RE ion, its radiative transition rate would need to be much greater than that of the red emission to compete and significantly contribute to the color mixing. A prime candidate for such a trap is a Si–Mg complex located close to a Eu^{3+} ion. This defect emits blue and has a sufficiently short radiative lifetime.[27,28] This defect has also been shown to result in Eu-doped GaN-based devices that also emit 430 nm blue light and where the ratio of blue to red light can be controlled through the current injection parameters.[23] New simulations are needed that explore more involved pulse sequences to allow for the independent manipulation of the m_1 population while keeping the $^5D_0$ to $^5D_1$ ratio constant. Furthermore, additional simulations and analysis could be used to check the frequency and intensity-dependent tunability across a more complete color space. In this way, these simulations help us to predict what types of structures could show potential for practical devices to achieve a fully tunable single-pixel LED.

ACKNOWLEDGMENTS

This study was supported by a grant from the National Science Foundation (No. NSF-ENG-ECCS 2129183).

AUTHOR DECLARATIONS

Conflict of Interest

The authors have no conflicts to disclose.

DATA AVAILABILITY

The data that support the findings of this study are available from the corresponding author upon reasonable request.

REFERENCES

[1]T. Han, V. Vaganov, S. Cao, Q. Li, L. Ling, X. Cheng, L. Peng, C. Zhang, A. N. Yakovlev, Y. Zhong, and M. Tu, Sci. Rep. **7**, 45944 (2017).
[2]I. Monostori, M. Heilmann, G. Kocsy, M. Rakszegi, M. Ahres, S. B. Altenbach, G. Szalai, M. Pál, D. Toldi, L. Simon-Sarkadi, N. Harnos, G. Galiba, and E. Darko, Front. Plant Sci. **9**, 605 (2018).
[3]E. S. Soliman and R. A. Hassan, Vet. World **12**, 1052 (2019).
[4]K. M. Zielinska-Dabkowska, Nature **553**, 274 (2018).
[5]J. Nie, Z. Chen, F. Jiao, C. Li, J. Zhan, Y. Chen, Y. Chen, X. Kang, Y. Wang, Q. Wang, W. Dang, W. Dong, S. Zhou, X. Yu, G. Zhang, and B. Shen, IEEE Photonics J. **11**, 1 (2019).
[6]D. Ferreira de Souza, P. P. Fernandes da Silva, L. F. A. Fontenele, G. D. Barbosa, and M. O. Jesus, Energy Rep. **5**, 409 (2019).
[7]P. M. Pattison, M. Hansen, and J. Y. Tsao, C. R. Phys. **19**, 134 (2018).
[8]J.-Il. Hwang, R. Hashimoto, S. Saito, and S. Nunoue, Appl. Phys. Express **7**, 071003 (2014).
[9]K. Chung, J. Sui, B. Demory, and P.-C. Ku, Appl. Phys. Lett. **111**, 041101 (2017).
[10]C.-M. Kang, S.-J. Kang, S.-H. Mun, S.-Y. Choi, J.-H. Min, S. Kim, J.-P. Shim, and D.-S. Lee, Sci. Rep. **7**, 10333 (2017).
[11]S. Baek, H. Kim, G. Lee, and S. Lee, Adv. Electron. Mater. **8**, 2100598 (2022).
[12]L. Yang, Y. Wang, H. Xu, W. Liu, C. Zhang, C. Wang, Z. Wang, J. Ma, and Y. Liu, ACS Appl. Mater. Interfaces **10**, 15812 (2018).
[13]H. Zhang, Q. Su, and S. Chen, Nat. Commun. **11**, 2826 (2020).
[14]Q. Wang, J. Bai, C. Zhao, M. U. Ali, J. Miao, and H. Meng, Appl. Phys. Lett. **118**, 253301 (2021).
[15]D. Braun, Synth. Met. **92**, 107 (1998).
[16]K. Kishino, N. Sakakibara, K. Narita, and T. Oto, Appl. Phys. Express **13**, 014003 (2020).

[17]F. Gou, E.-L. Hsiang, G. Tan, Y.-F. Lan, C.-Y. Tsai, and S.-T. Wu, Crystals **9**, 39 (2019).
[18]Z. Wang, X. Shan, X. Cui, and P. Tian, J. Semicond. **41**, 041606 (2020).
[19]S.-J. Park, S.-H. Song, S. S. Kim, and J.-K. Song, Small **17**, 2007397 (2021).
[20]H. S. El-Ghoroury, Y. Nakajima, M. Yeh, E. Liang, C.-L. Chuang, and J. C. Chen, Opt. Express **28**, 1206 (2020).
[21]U. Hömmericha, E. E. Nyein, D. S. Lee, J. Heikenfeld, A. J. Steckl, and J. M. Zavada, Mater. Sci. Eng. **105**, 91 (2003).
[22]S. Ichikawa, K. Shiomi, T. Morikawa, D. Timmerman, Y. Sasaki, J. Tatebayashi, and Y. Fujiwara, Appl. Phys. Express **14**, 031008 (2021).
[23]B. Mitchell, R. Wei, J. Takatsu, D. Timmerman, T. Gregorkiewicz, W. Zhu, S. Ichikawa, J. Tatebayashi, Y. Fujiwara, and V. Dierolf, ACS Photonics **6**, 1153 (2019).
[24]B. Mitchell, H. Austin, D. Timmerman, V. Dierolf, and Y. Fujiwara, Nanophotonics **10**, 851 (2020).
[25]D. Timmerman, Y. Matsude, Y. Sasaki, S. Ichikawa, J. Tatebayashi, and Y. Fujiwara, Phys. Rev. Appl. **14**, 064059 (2020).
[26]B. Mitchell, V. Dierolf, T. Gregorkiewicz, and Y. Fujiwara, J. Appl. Phys. **123**, 160901 (2018).
[27]D.-g. Lee, R. Wakamatsu, A. Koizumi, Y. Terai, and Y. Fujiwara, Jpn. J. Appl. Phys. **52**, 08JM01 (2013).
[28]Y.-H. Kwon, S. K. Shee, G. H. Gainer, G. H. Park, S. J. Hwang, and J. J. Song, Appl. Phys. Lett. **76**, 840 (2000).
[29]R. Wei, B. Mitchell, D. Timmerman, T. Gregorkiewicz, W. Zhu, J. Tatebayashi, S. Ichikawa, Y. Fujiwara, and V. Dierolf, Phys. Rev. B **100**, 081201(R) (2019).
[30]D. Timmerman, B. Mitchell, S. Ichikawa, M. Nagai, M. Ashida, and Y. Fujiwara, Phys. Rev. B **101**, 245306 (2020).
[31]Y. Robin, F. Hemeret, G. D'Inca, M. Pristovsek, A. Trassoudaine, and H. Amano, Jpn. J. Appl. Phys. **58**, SCCC06 (2019).
[32]B. Mitchell, D. Timmerman, J. Poplawsky, W. Zhu, D. Lee, R. Wakamatsu, J. Takatsu, M. Matsuda, W. Guo, K. Lorenz, E. Alves, A. Koizumi, V. Dierolf, and Y. Fujiwara, Sci. Rep. **6**, 18808 (2016).
[33]S. Khromov, C. G. Hemmingsson, H. Amano, B. Monemar, L. Hultman, and G. Pozina, Phys. Rev. B **84**, 075324 (2011).
[34]B. Mitchell, D. Timmerman, W. Zhu, J. Y. Lin, H. X. Jiang, J. Poplawsky, R. Ishii, Y. Kawakami, V. Dierolf, J. Tatebayashi, S. Ichikawa, and Y. Fujiwara, J. Appl. Phys. **127**, 013102 (2020).